JOURNAL OF Applied Polymer SCIENCE

Formation of an Interconnected Lamellar Structure in PVDF Membranes with Nanoparticles Addition via Solid-Liquid Thermally Induced Phase Separation

Wenzhong Ma,[1] Jun Zhang,[2] Bart Van der Bruggen,[3] Xiaolin Wang[1]

[1]Department of Chemical Engineering, Beijing Key Laboratory of Membrane Materials and Engineering, Tsinghua University, Beijing 100084, China

[2]Department of Polymer Science and Technology, College of Materials Science and Engineering, Nanjing University of Technology, Nanjing 210009, China

[3]K.U. Leuven, Department of Chemical Engineering, Laboratory for Applied Physical Chemistry and Environmental Technology, B-3001 Leuven, Belgium

Correspondence to: X. Wang (E-mail: xl-wang@tsinghua.edu.cn)

ABSTRACT: Novel microporous membranes were prepared via thermally induced solid-liquid (S-L) phase separation of mixtures containing poly(vinylidene fluoride) (PVDF)/diphenyl ketone (DPK)/nanoparticles [such as montmorillonite (MMT) and polytetrafluoroethylene (PTFE)] in diluted systems with a mass ratio of 29.7/70/0.3 wt %. The crystallization and melting characteristics of these diluted systems were investigated by polarizing optical microscopy (POM), scanning electron microscopy (SEM), differential scanning calorimetry (DSC), Fourier transform infrared spectroscopy (FTIR), and wide angle X-ray diffraction (WAXD). The nanoparticle structure and the interaction between PVDF chains and nanoparticle surfaces determined the crystallization behavior and morphology of the PVDF membrane. The addition of MMT and PTFE had a significant nucleation enhancement on the crystallization of PVDF accompanied by S-L phase separation during the thermally induced phase separation (TIPS) process. It was observed that an interconnected lamellar structure was formed in these two membranes, leading to a higher tensile strength compared with that of the reference membrane without nanoparticles addition. Additionally, addition of MMT facilitates the fiber-like β phase crystal formation, resulting in the highest elongation at break. © 2012 Wiley Periodicals, Inc. J. Appl. Polym. Sci. 000: 000–000, 2012

KEYWORDS: poly(vinylidene fluoride); crystallization; nanoparticles; thermally induced phase separation; membrane structure

Received 27 September 2011; accepted 27 February 2012; published online
DOI: 10.1002/app.37574

INTRODUCTION

Poly(vinylidene fluoride) (PVDF), a semicrystalline polymer with excellent physical and chemical properties and a good thermal stability, has been often used in synthesis of porous membranes. Highly porous PVDF membranes have been extensively prepared by phase separations of the polymer solution that can be produced by several methods, including immersion precipitation,[1] vapor-induced phase separation,[2] and thermally induced phase separation (TIPS).[3,4] Most authors prepared PVDF membranes through immersion precipitation (non-solvent induced phase separation, i.e., NIPS). However, this method usually yields asymmetric membranes with a finger-like structure of the skin layer near the surface, which results from a fast exchange between the solvent and the non-solvent. In contrast, TIPS method has been proven to be an essential method for making commercial membranes because of the advantages over membrane preparation by others (such as less control parameters, effective control of the membrane structure).[3,4] The TIPS process begins with dissolution of polymer and diluent (having a high boiling point). Then the solution is cast or extruded into a desired shape and cooled to induced phase separation accompanying with a solidification of the polymer. A microporous membrane can be obtained after the diluent is extracted by another solvent and this extractant is completely evaporated.[5] As for the TIPS mechanism, a solid-liquid (S-L) phase separation and a liquid-liquid (L-L) phase separation followed by polymer crystallization or glass transition is used, which offers a great flexibility in controlling the microscopic morphology of polymeric systems.[3–7] This method can be applicable to a wide range of polymers including those polymers that cannot be formed into

membranes via NIPS because of solubility problems, such as polypropylene (PP),[8] polyethylene (PE),[9] poly (4-methyl-pentene) (TPX),[10] and poly(ethylene chlorotrifluoroethylene) (ECTFE).[11] Commonly, PVDF/diluent systems undergo an S-L phase separation associated with the crystallization of PVDF, owing to the strong interactions between the PVDF chain and the diluents molecule. In this way, a spherulitic morphology with irregular pores in the spherulites is formed, often including large macrovoids.[12–14] This kind of membrane structure would have a poor mechanical strength because there is no interconnection between the spherulites. Recently, Lanceros-Méndez's coworkers[15,16] has proved that the morphology variations and porosity depending on the solvent evaporation rate when PVDF crystallized from solutions, which implies that when phase separation occurs, the kinetic parameters (including quenching temperatures, the time limit for each phase separation region) will play an important role on the ultimate membrane structures.

To obtain a bicontinuous membrane structure and to avoid a spherulitic membrane structure to be formed via the S-L phase separation, a diluent can be applied, which eventually can induce an L-L phase separation. Lately, it has been found that a L-L phase separation can be obtained in PVDF/diphenyl ketone (DPK) and diphenyl carbonate systems in a wide range of polymer concentrations.[17,18] Depending on the PVDF concentration in the solution, L-L phase separation proceeds in different mechanisms.[19] As illustrated by the membrane performance,[17,18] a bicontinuous pore structure but poor mechanical properties were obtained, because the L-L phase separation occurred when the polymer concentration was in the low range. Some researchers incorporated amorphous poly(methyl methacrylate) (PMMA) into PVDF diluted systems and a short L-L phase separation region was obtained.[20,21] In a U.S. patent,[22] the inventor applied a powdery hydrophobic silica as an inorganic filler to PVDF diluted system in which dibutyl phthalate (DBP), dioctyl phthalate (DOP), or mixtures of them were used as diluents. By the TIPS process, a porous membrane having a uniform, three-dimensional, network pore structure, and having excellent mechanical strength was produced after extracting the organic liquid and the powdery hydrophobic silica. The acceptable residual ratio of the hydrophobic silica is preferably not higher than 1 vol %, based on the volume of the final membrane structure. Li and Lu[23] investigated blended films prepared from a ternary mixture of PVDF/$CaCO_3$/DBP via TIPS, and there was no formation of interconnected pores; also the morphologies presented a regular, large, spherulitic structure. The reason why the PVDF membrane prepared via the TIPS process has a different structure when inorganic particles are added into the solution remains unclear.

Our previous work[24,25] showed that two types of nanoparticles have different extents of nucleation enhancement to the crystallization of PVDF. As demonstrated, a small amount of nanoparticles (1.0 wt %) has a remarkable enhancement on the crystallization and affects the morphology of crystals. The aim of this work is to investigate the effect of a small amount of nanoparticles added to the diluted system on the mechanism of S-L phase separation and crystallization of PVDF during the TIPS process. Furthermore, it was attempted to obtain membranes with a structure of interconnected networks of crystallites.

EXPERIMENTAL

Materials

PVDF (Kynar K-761), in powder form, was supplied by Elf Atochem of North America. Commercial grade nanoparticles of montmorillonite clay (MMT) and polytetrafluoroethylene (PTFE) were used. Each material was used as received without purification.

Sample Preparations

PVDF/DPK/nanoparticles mixtures with a mass ratio of 29.7/70/0.3 wt % were prepared by using a mini twin-screw extruder (ULTnano TW05, Technovel Corporation, Japan). The rate of screwing was 120 rpm, the processing temperature of the extruder was set at 170, 200, 230, and 230°C from the hopper to the die, and the residence time was 10 min. In all these mixtures, the DPK content was fixed at 70 wt % and the mass ratio of PVDF and nanoparticles was fixed at 29.7/0.3 (=99/1) wt/wt. At this diluent concentration, only the S-L phase separation would occur during the TIPS process.[26] Previous work also showed that a small amount of nanoparticles (1.0 wt %) in the PVDF matrix has a remarkable enhancement on the crystallization and affects the morphology of crystals.[24,25] So, choosing PVDF/DPK/nanoparticles mixtures with a mass ratio of 29.7/70/0.3 wt %, we can clearly investigate the effect of nanoparticles addition on the crystallization of PVDF and the membrane structure during the TIPS process.

PVDF membranes with or without nanoparticles addition were prepared by the following procedure. The solid sample (PVDF/nanoparticles/DPK mixture) was chopped into small pieces and placed between a pair of microscope cover slips, as described elsewhere.[27] They were heated in an oven at 180°C for 5 min. Subsequently, they were quenched from the melt to the water bath at 25°C till complete solidification. Mixtures with approximately the same thickness of 0.2 mm were achieved throughout the TIPS process. After recovery from the slips, the mixtures were immersed in ethanol for 48 h to extract the diluent. Eventually, microporous PVDF membranes with or without nanoparticles addition were obtained after complete volatilization of ethanol.

Characterization Techniques

Wide angle X-ray diffraction (WAXD) was done in a Bruker D8-Advance diffractometer (Cu K_α radiation, 40 kV and 40 mA). The scanning angle ranged from 5 to 50° with scanning velocity of 4°/min. The samples for this measurement were PVDF membranes with or without nanoparticles addition, from which the DPK had been extracted by ethanol.

Fourier transform infrared spectroscopy (FTIR) spectra were obtained by using a Nicolet 6700 with 4 cm^{-1} resolution, 64 scans. FTIR-attenuated total reflection (ATR) spectra were applied in this work. The samples used were the same as those for WAXD measurement.

Differential scanning calorimetry (DSC) analyses were made on a TA Instruments Q-200 differential scanning calorimeter in a dry nitrogen atmosphere. For a sample measurement, about 10 mg of PVDF/DPK-diluted mixtures with or without nanoparticles was sealed into an aluminum pan. Before the melting tests, the thermal history was erased by a quick heating to

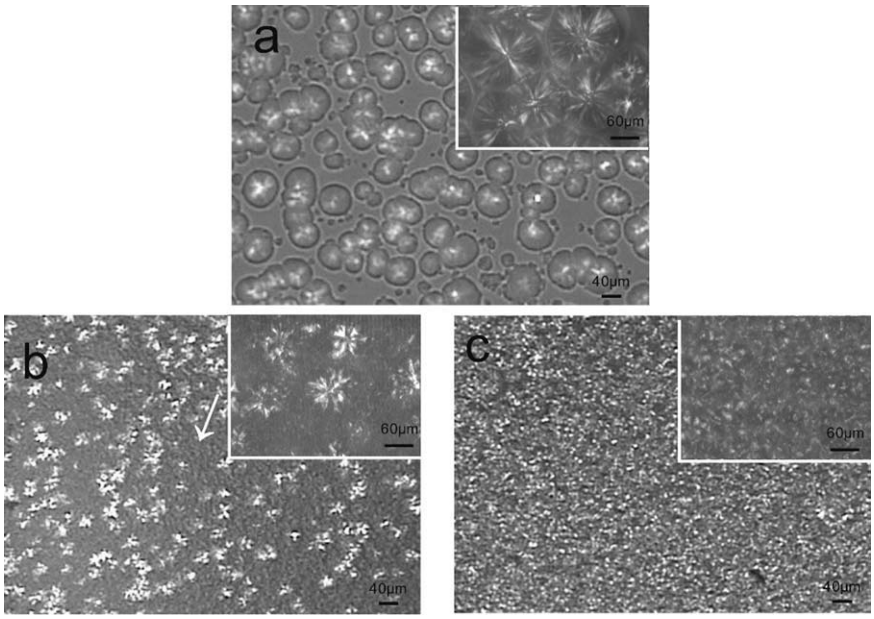

Figure 1. Polarized optical micrographs showing the spherulitic morphology of PVDF/DPK-diluted mixtures with or without nanoparticles crystallized after full solidification from the melt state at 2°C/min: (a) without nanoparticles; (b) MMT; and (c) PTFE.

200°C. Then, the crystallization curve was obtained at a cooling rate of 10°C/min to 40°C. After maintaining at 40°C for 2 min, the mixtures were heated up to 200°C at a rate of 10°C/min. The crystallinity of PVDF (X_c) was calculated as in previous work.[12,28] In the modulated DSC (MDSC) mode with MDSC option and a refrigerated cooling system (RCS), the nitrogen flow was 50 ml/min, the heating rate was 2°C/min or lower, the modulation period was 60 s and the amplitude was ±0.21-0.24°C. The combination of heating rate and period was always chosen so that there were at least four modulation cycles during the transition of interest.

The morphology development of spherulites, which appear as bright areas under polarized light in the dark background of neat PVDF and PVDF/nanoparticles/DPK mixtures were observed under cross polariers using a polarizing microscope (Olympus BX 51) equipped with a temperature controller (Linkam THMS 600). A thin slice was cut from the mixture, inserted between two microscope slides (with diameter of 20 mm), melted up to 200°C, and kept at this temperature for 5 min to erase the thermal history of the sample. Then, it was cooled down to 50°C at a slow rate of 2.0°C/min. Photomicrographs of growing spherulites were taken when the crystallization was completely finished.

PVDF membranes with or without nanoparticles addition were fractured in liquid nitrogen, and the surfaces were sputtered with Au in vacuum. Then, the scanning electron micrographs (SEM) of dried and gold-coated cross-sections were taken with a JEOL JSM-7401 instrument.

The tensile strength of the resulting PVDF membranes with or without nanoparticles addition were measured by a universal testing machine (Shimadzu AGS-100A) equipped with a 5 kg load cell. Before the test, the membranes with 0.2 mm thickness were cut into 10 × 3 mm^2 strips. The cross-head speed was controlled at 2 mm/min. An average value of the tensile strength was calculated by measuring three samples for each batch of the membranes.

RESULTS AND DISCUSSION

Optical Morphology of PVDF/DPK-Diluted Mixtures with or Without Nanoparticles

It is known that a PVDF/DPK mixture with 30 wt % PVDF concentration undergoes an S-L phase separation in the TIPS process.[17,26] Addition of 1.0 wt % nanoparticles into the PVDF matrix was found to enhance the nucleation effect remarkably. In the DPK-diluted mixture, the enhanced nucleation effect led to numerous small PVDF crystals when the nanoparticles were added at the beginning of the phase separation. Figure 1 shows the typical spherulitic texture of the PVDF/DPK-diluted mixture with or without nanoparticles addition when cooling from the melt state under the slowly cooling circumstance (2°C/min). In the DPK-diluted mixture without nanoparticles, large size spherulites were observed. When nanoparticles were incorporated into the DPK-diluted mixture, obviously more and smaller spherulites were formed. As seen from Figure 1(b,c), the obtained PVDF spherulite size is dramatically decreased with those nanoparticles incorporation.

Because of strong interactions between the nanoparticle surface and the PVDF chain exist in the MMT addition mixture, an area with a dark region where undiscerned crystals are formed [as denoted in Figure 1(b)] was observed. This indicates that MMT addition not only facilitates formation of smaller spherulites but also favors a fiber-like structure formation (lacks birefringence), which is due to the strong interactions between the surface of MMT and PVDF chains. When MMT was added, an intercalation of PVDF chains into silicate galleries could occur.[29] Thus, when the S-L phase separation began, two kinds of PVDF

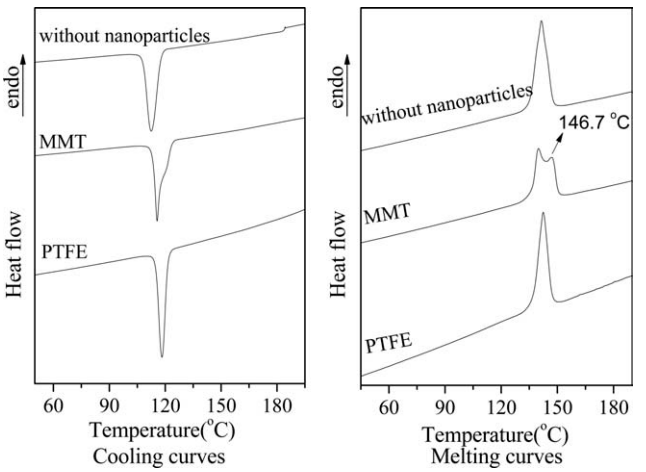

Figure 2. DSC scans of crystallization and melting traces for PVDF/DPK-diluted mixtures with or without nanoparticles.

crystals were formed: (1) small spherulites in which MMT particles act as the nuclei; (2) a PVDF fiber-like structure formed between MMT layers. As for the mixture with PTFE addition, more uniform spherulites were formed, which indicates the excellent nucleation effect on the PVDF crystals.

Thermal Analyses of PVDF/DPK-Diluted Mixtures with or Without Nanoparticles

DSC scans, including the crystallization of PVDF/DPK-diluted mixtures with or without nanoparticles at a cooling rate of 10°C/min when cooling from 200°C and subsequent melting behavior at a heating rate of 10°C/min to 200°C, respectively, are shown in Figure 2. The corresponding results from the DSC measurement are summarized in Tables I and II, respectively.

In the crystallization curves (Figure 2), the crystallization peak shifts to a higher temperature for each mixture to which nanoparticles were added. This indicates that these nanoparticles can reduce the initial energy barrier for crystallization of PVDF, so the crystallization of PVDF in the DPK-diluted mixture occurs at higher temperature. The detailed crystallization results from the crystallization curves are summarized in Table I. The crystallization temperatures of mixtures to which nanoparticles were added (including the values of T_c^{on}, T_c^p, and T_c^f) are higher than those of the mixture without nanoparticles addition. The difference between the onset and peak crystallization temperature ΔT_c obtained from the mixture with PTFE addition is smaller than that of the mixture without nanoparticles, except of that obtained from the mixture with the MMT addition. The crystallization half-time ($t_{1/2}$) was also obtained from the crystallization curves. As shown in Table I, $t_{1/2}$ is much lower for the PTFE addition mixture than when no nanoparticles were added, except for the MMT addition mixture. These results confirm that MMT would be the most excellent nucleating agent for PVDF, which agrees with the work of Schneider et al.[30]

As for the MMT addition mixture, the values of ΔT_c and $t_{1/2}$ are even higher than those for the one without nanoparticles addition. A shoulder peak in the crystallization curve for the MMT addition mixture was observed (Figure 2). The MMT nanoparticles in the PVDF matrix were found to act as an effective nucleation agent[27]; on the other side, because of the spatially hierarchical structure for MMT nanoparticles, PVDF chains could penetrate into silicate galleries, resulting in the restricted movement of the PVDF chain and leading to suppression of the crystallization.[31,32] Combining these two effects, the reduced crystallization rate can be understood.

In the melting curves of DPK-diluted mixtures with PTFE nanoparticles addition, only one melting peak was observed (Figure 2). However, two melting peaks were obtained in the MMT addition mixture. As illustrated by polarizing optical microscopy (POM) results (Figure 1), small and uniform spherulites were observed in the mixture with addition of PTFE, which indicates that only the nucleation effect is presented in this mixture. As for the mixture with MMT addition, except for this kind of nucleation effect, there could be different crystalline forms of PVDF crystals in it. Table II summarizes the detailed melting results obtained in Figure 2. As for these diluted mixtures with nanoparticles addition, the onset of the melting temperatures (T_m^{on}) is increased to a higher level. The peak melting temperatures (T_m^p) and the final melting temperatures (T_m^f) for PTFE addition mixtures are almost not changed. As for the mixture with MMT addition, the lower melting peak is close to others, but the value T_m^f shifts up to a higher temperature. The degree of the homogeneity for PVDF crystal size, which is indicated by a difference of ΔT_m ($\Delta T_m = T_m^f - T_m^{on}$), was obtained. The higher ΔT_m is, the more uniform crystal size is obtained. As shown in Table II, the homogeneity of the crystal size of PVDF in the DPK-diluted mixtures with PTFE is better than that in the mixture without nanoparticles, except that for the mixture with MMT addition. This can be attributed to the remarkable nucleation effect in the mixture with PTFE addition, which is confirmed by the result obtained in POM and crystallization behavior aforementioned. As for the MMT addition mixture, because of the double melting peaks in the melting curve, ΔT_m is even larger than that of the mixture without nanoparticles (Figure 2). In addition, ΔH_m (proportional to the crystallinity of the blends) for the diluted mixtures with MMT and PTFE nanoparticles is higher than in the mixture without nanoparticles. This implies that addition of nanoparticles into the PVDF/DPK-diluted mixture favors the crystallization.

The same double melting phenomenon was also observed for PVDF/MMT nanoparticles composites when heating to the

Table I. DSC Crystallization Results of PVDF/DPK-Diluted Mixtures with or Without Nanoparticles

DPK-diluted mixtures	T_c^{on} (°C)	T_c^p (°C)	T_c^f (°C)	ΔT_c (°C)	ΔH_c (J g^{-1})	$t_{1/2}$ (min)
Without nanoparticles	118.1	112.3	107.9	5.8	17.4	0.32
With MMT	123.6	115.6	113.4	8.0	18.2	0.33
With PTFE	121.4	118.3	115.0	3.1	20.3	0.23

T_c^{on}, onset crystallization temperature of PVDF; T_c^p, peak crystallization temperature of PVDF; T_c^f, final crystallization temperature of PVDF; $\Delta T_c = T_c^{on} - T_c^p$; ΔH_c, crystallization enthalpy of PVDF.

Table II. DSC Melting Results of PVDF/DPK-Diluted Mixtures with or Without Nanoparticles

DPK-diluted mixtures	T_m^{on} (°C)	T_m^p (°C)	T_m^f (°C)	ΔT_m (°C)	ΔH_m (J g^{-1})	X_c (%)
Without nanoparticles	134.9	141.1	147.2	12.3	17.1	54.5
With MMT	136.3	140.0[a]	150.4	14.1	18.5	59.6
With PTFE	137.0	142.4	147.3	10.3	19.9	64.1

T_m^{on}, onset melting temperature of PVDF; T_m^p, peak melting temperature of PVDF; T_m^f, final melting temperature of PVDF; $\Delta T_m = T_m^f - T_m^{on}$, ΔH_m, melting enthalpy; X_c, crystallinity of PVDF.
[a]This melting peak temperature is the lowest one in the melting curve.

melt. It has been demonstrated that this result was due to the melting and recrystallization behavior. However, in the diluted mixture, the DPK dilution effect would result in both imperfect and perfect crystals as a result of the crystallization of PVDF during the TIPS process, leading to the double melting peaks in the heating curves.[33] To identify whether the melting and recrystallization occurred or not in the diluted mixture with MMT addition, MDSC was performed. MDSC applies a sinusoidal modulation (oscillation) on the conventional linear heating or cooling ramp[34] and makes the total heat flow to be separated into the heat capacity component or reversing heat flow and the kinetic component or non-reversing heat flow. Herein, the experimental parameters are chosen to provide a heat-isothermal modulated heating rate profile. The mixtures for MDSC measurements were the same as the ones used in the DSC heating tests (heating to 200°C at a heating rate of 10°C/min). Thus, the kinetic process of recrystallization during heating can thus be verified from the non-reversing heat flows. The total, reversing, and non-reversing heat flows for the MDSC experiment of PVDF/DPK-diluted mixtures with or without nanoparticles are plotted in Figure 3. The MDSC heat flow curves (including the total, reversing, and non-reversing ones) for PVDF/DPK-diluted mixtures with or without nanoparticles (except for the MMT addition mixture) have two melting peaks, which locate at 138.9 and 146.3°C, respectively (Figure 3). As given by the conventional DSC results, only one melting peak with a peak temperature ranging from 140.0 to 142.4°C was obtained (Table II), which locates between 138.9 and 146.3°C. This is reasonable in the sense that with the relatively low heating rate in MDSC scans (~ 1.5°C/min), a subtle melting behavior was detected. Double melting peaks in the MDSC curves may be due to the different degrees of perfection for PVDF crystals. In the non-reversing heat flow curves, there are only endothermal peaks for all these diluted mixtures, which indicate that no recrystallization occurred during the heating process.

Additionally, the total melting enthalpy obtained from MDSC (sums of reversing and non-reversing) is very close to that obtained from conventional DSC. The melting enthalpy of the reversing part for the nanoparticles addition mixtures is very close to that for the mixture without nanoparticles, but the melting enthalpy of the non-reversing part is higher than that for the mixture without nanoparticles. This indicates more imperfect crystals formed in the nanoparticles addition mixtures. However, it is interesting to notice that the MMT addition mixture has the highest ΔH_m obtained from the non-reversing heat flow, but the lowest one obtained from the reversing heat flow is totally different from that of mixtures with or without nanoparticles. This obviously confirms that the crystals formed in the MMT addition mixture have more imperfect regions, which suggests the more evident restricted effect on the crystal growth in this mixture.

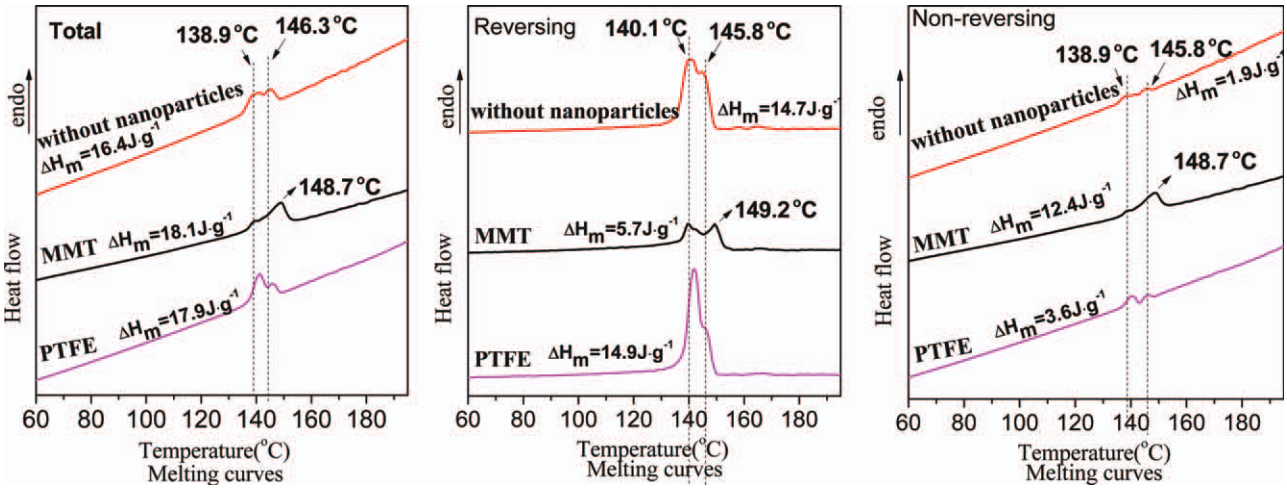

Figure 3. MDSC heat flow traces of PVDF/DPK-diluted mixtures with or without nanoparticles after cooling from the melt to the 40°C at 10°C/min, including total heat flow, reversing heat flow, and non-reversing heat flow. [Color figure can be viewed in the online issue, which is available at wileyonlinelibrary.com.]

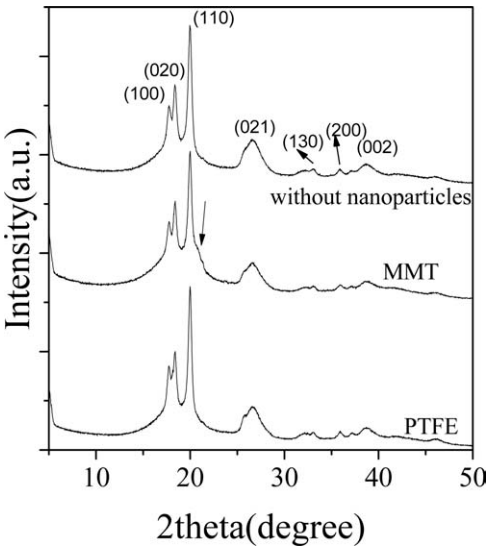

Figure 4. X-ray diffractograms of PVDF membranes with or without nanoparticles.

WAXD Analysis of PVDF Membranes with or Without Nanoparticles

To confirm the crystalline phase in the PVDF membranes with or without nanoparticles, X-ray diffraction was performed (Figure 4). The peaks at $2\theta = 17.75$, 18.36, 19.96, 26.58, 33.10, 36.99, and 39.00° in the curve for the neat PVDF membrane [Figure 4(a)] represent the diffractions in planes (100), (020), (110), (021), (130), (200), and (002), respectively, which are all characteristic of the α phase of PVDF.[35,36] This confirms that there are predominant α phase crystals in the PVDF/DPK-diluted mixtures with or without nanoparticles. As shown in Figure 4, the predominant diffraction peak for the α phase ($2\theta = 19.96°$) in the PTFE addition membrane is sharper (in width) than that in the membrane without nanoparticles addition. This indicates that the amount of nanoparticles addition favors the uniform size PVDF crystals formation because of the nucleation effect. As for the MMT addition membrane, there is a shoulder peak near $2\theta = 21°$ (denoted by the arrow in Figure 4); this may indicate the presence of β phase of PVDF in this membrane, i.e., both α and β phase could exist in the MMT addition membrane.

IR Spectroscopy

To confirm the crystalline phase of PVDF in the membranes, IR spectra (in ATR mode) of PVDF membranes with or without nanoparticles were taken, as shown in Figure 5. The PVDF membrane with PTFE addition or without nanoparticles addition has well-defined absorption bands at 1423, 1400, 1383, 1211, 1149, 1069, 975, 872, 854, 794, and 763 cm^{-1}. As reported, these IR absorption bands represent the characteristic spectrum of the α phase of PVDF crystal.[35,37] It indicates that only the crystallization of α phase PVDF predominates in the crystallization in these membranes, which agrees with the result of Gregorio and Nociti.[38] However, with regard to the membrane with MMT addition, except for the absorption bands of the α phase PVDF, an additional absorption band at 840 cm^{-1}, which is characteristic of the β phase of PVDF, was observed. So, the double peaks are associated with two distinct crystals or morphologies, i.e., there is β phase crystal formed, and the upper peak should be attributed to the melting phase, because the melting peak temperature of the β phase PVDF crystal is higher than that of the α phase crystal.[35,39–41] The presence of the β phase could be due to the matching of the crystal lattice of the nanoclay with that of the PVDF β phase.[42] As reported in the work of Ramasundaram et al.,[43] the ion-dipole interaction between the exfoliated clay nanolayers and PVDF is a main factor for the formation of β-phase.

The relative amount of the β-PVDF in the membrane sample with MMT addition was calculated applying a previously developed method, which is as follows[40,44]:

$$F(\beta) = \frac{A_\beta}{1.3\,A_\alpha + A_\beta} \tag{1}$$

where A_α and A_β are the absorbance in FTIR spectrum corresponding to 763 and 840 cm^{-1} bands, respectively. As calculated by eq. (1), the relative amount of β-PVDF in the membrane with MMT addition is 28.5%.

Equilibrium Melting Point Calculation of PVDF/DPK-Diluted Mixtures with or Without Nanoparticles

The equilibrium melting temperature of the polymer, as one of the crystal parameters which efficiently affect the TIPS process, was determined by the Hoffman-Weeks extrapolation method.[45] Lee et al.[46] simplified the Hoffman-Weeks equation as follows to calculate the equilibrium melting point of the mixture:

$$T_m = \eta T_c + (1-\eta)T_m^0 \tag{2}$$

The equilibrium melting temperature T_m^0 is obtained from the intersection of this line with $T_m = T_c$. A value of $\eta < 1$ implies that the crystals are perfectly stable or not, whereas a value of $\eta = 1$ reflects inherently unstable crystals.

As demonstrated,[6] with an increase of the melting temperature T_m^0 for semicrystalline polymer solution, the crystalline curve

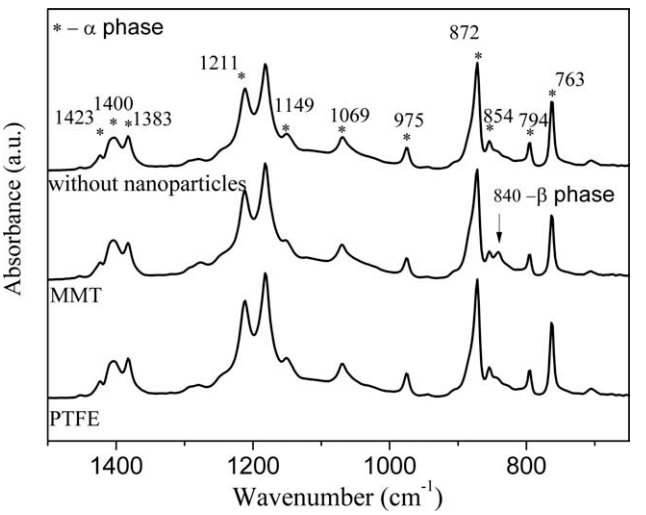

Figure 5. IR spectra of PVDF membranes with or without nanoparticles.

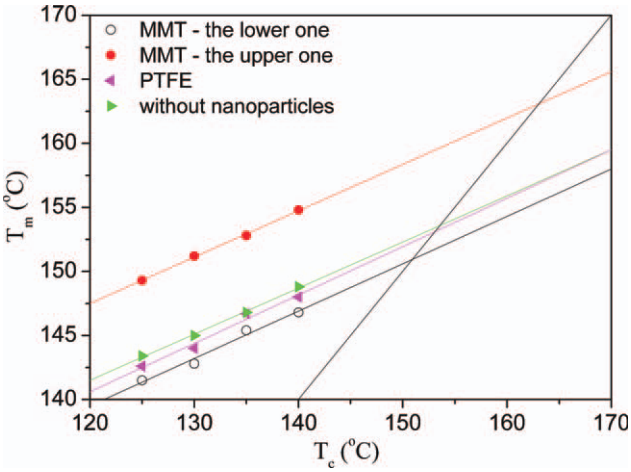

Figure 6. Hoffman-Weeks plot for PVDF/DPK mixtures with or without nanoparticles (crystallization time = 4 h): ▶) without nanoparticles; ●) MMT; and ◀) PTFE. [Color figure can be viewed in the online issue, which is available at wileyonlinelibrary.com.]

(i.e., the bottom line for L-L phase separation or the boundary line for S-L phase separation) would shift to a higher level. In addition, the value of T_m^0 for the PVDF/DPK-diluted mixture increases with an increase in the polymer concentration.[26] The driving force for crystallization, i.e., T_m^0-T_c (T_c is the crystallization temperature), is dominated by the change of T_m^0, if the crystallization temperature (i.e., quenching temperature in this work) is fixed. The higher of T_m^0, the higher driving force will be obtained. Thus, the driving force for the phase separation will be influenced by T_m^0. In this work, the polymer concentration is 29.7 wt %, which is near the monotectic point (30 wt % PVDF[26]), so the crystallization effect of PVDF would be a predominant factor when the S-L phase separation occurs during TIPS process. T_m as a function of crystallization temperature T_c for the PVDF/DPK-diluted mixtures with or without nanoparticles is shown in Figure 6. The obtained values of T_m^0 and η are given in Table III. Straight lines were drawn and a depression of T_m for the same T_c was observed, except for the one derived from the upper melting peak in the diluted mixture with MMT addition, which indicates an increase of the number of defects between PVDF lamellae because of the nucleation effect. Compared with that of the diluted mixture without nanoparticles, the slope η of PVDF in DPK with addition of MMT and PTFE nanoparticles is somewhat higher. This indicates that more unstable crystals (having thinner lamellar thickness) are formed in the mixture with addition of MMT and PTFE nanoparticles. The value of T_m^0 obtained from the upper melting peak in the MMT addition mixture is much higher than that obtained in the mixture without nanoparticles. As discussed above, both α

Table III. Results of the Hoffman-Weeks Analysis of the PVDF/DPK-Diluted Mixtures with or Without Nanoparticles

DPK-diluted mixtures	T_m^0 (°C)	η
Without nanoparticles	153.6	0.36
With MMT	163.1[a]	0.36
	151.0[b]	0.37
With PTFE	153.0	0.38

[a]Values obtained from the upper melting peaks., [b]Values obtained from the lower melting peaks.

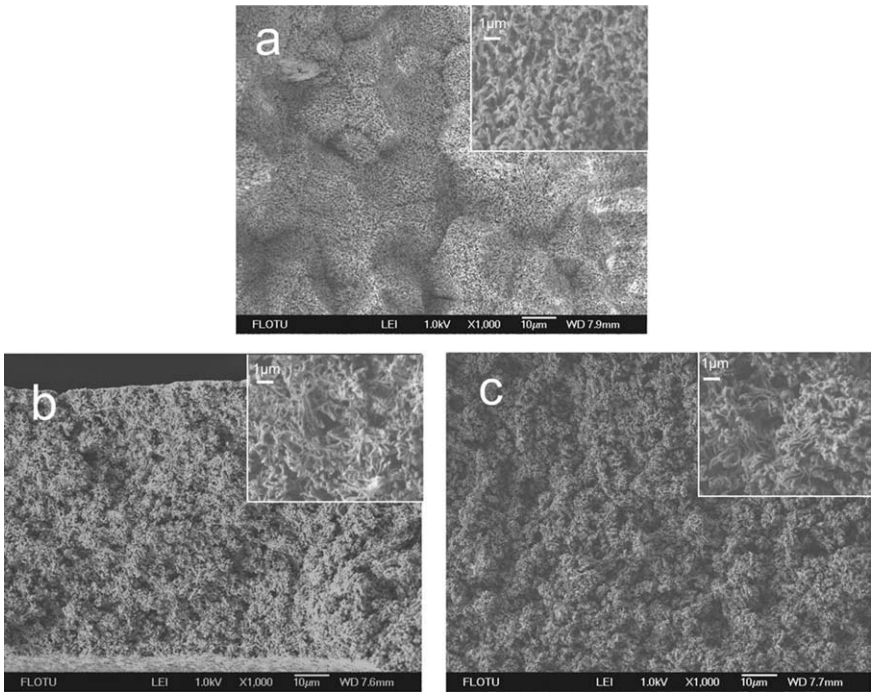

Figure 7. Cross-sections of PVDF membranes with or without nanoparticles obtained by quenching from the melt to the water bath at 25°C: (a) without nanoparticles; (b) MMT; and (c) PTFE.

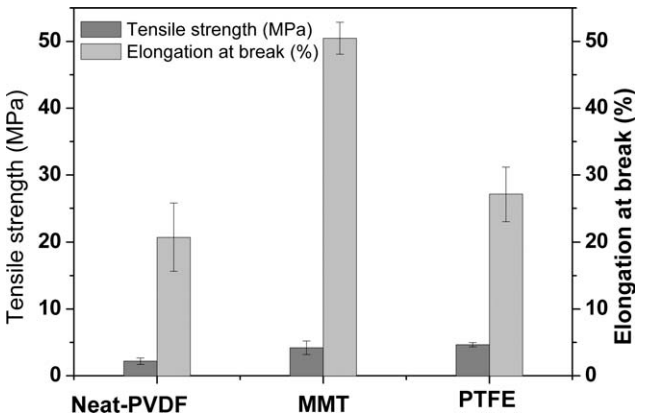

Figure 8. Tensile strength (error bars ± 1 S.D.) and elongation at break (error bars ± 5 S.D.) for PVDF membranes with or without nanoparticles obtained by quenching from the melt to the water bath at 25°C.

and β phase coexist in the MMT addition mixture. The highest value of T_m^0 could be ascribed to the β phase of PVDF crystals.

Structure and Tensile Strength of Membranes Derived from Mixtures of PVDF/DPK with or Without Nanoparticles Addition

Figure 7 shows the cross-sections of the membranes obtained from PVDF/DPK-diluted mixtures with or without nanoparticles by quenching from the melt to the water bath at 25°C. The membrane without nanoparticles addition forms impinged spherulites with largest size. It is suggested that the obvious S-L phase separation occurred during the quenching process, accompanying the rejection of diluent by the fast crystallization of PVDF, leading to small pores in the spherulites. The formation of a spherulitic structure in Figure 7 can be explained by the occurrence of the S-L phase separation via nucleation and growth of the PVDF in the quenching process. Because of the close T_m^0 for these diluted samples with or without nanoparticles addition, the crystallization driving force[47] should be the same when quenching from the melt to the water bath. So, the nucleation effect is predominant, which affects the crystallization of PVDF when the S-L phase separation occurs for the mixtures with nanoparticles addition. Obviously, the pore size obtained from the membranes with nanoparticles is nearly the same, but smaller than that obtained from the one without nanoparticles. This can be attributed to the short time for the S-L phase separation owing to the fast crystallization of PVDF. Both of MMT and PTFE nanoparticles addition membranes illustrate the lamellar crystal structure. This again confirms that MMT and PTFE nanoparticles have stronger interactions with PVDF chains and perform the best nucleation effect, resulting in the interconnected lamellar structure.

Figure 8 shows the tensile strength and elongation at break of PVDF membranes obtained by quenching the DPK-diluted mixtures with or without nanoparticles into the water bath (25°C). The tensile strength and elongation at break for the PVDF membrane without nanoparticles is 2.18 MPa and 20.73%, respectively. As for the MMT and PTFE addition membranes, the tensile strength is increased to 4.22 and 4.66 MPa, respectively, whereas the elongation at break for these two membranes is higher, compared with that for the one without nanoparticles. These results can be attributed to the structural and morphological changes induced by the addition of nanoparticles. As illustrated above, MMT and PTFE nanoparticles are the best nucleation agents for PVDF. Their addition results in the smallest spherulites and an even lamellar structure in the membrane. This interconnected structure leads to a much more conductive plastic flow under applied stress, thereby delaying crack formation. Thus, the tensile strength and elongation at break are higher than the membrane without nanoparticles. In addition, because of the spatial interactions between PVDF and MMT clay nanolayers, β-PVDF was formed, which give rise to a more efficient energy-dissipation mechanism in the membrane.[42] So, the membrane with MMT addition has a higher elongation at break than the one with PTFE addition.

CONCLUSIONS

The crystallization behavior of PVDF/DPK/nanoparticles (MMT and PTFE) diluted mixtures with a mass ratio of 29.7/70/0.3 wt % via thermally induced solid-liquid (S-L) phase separation was investigated. The nanoparticle structure and the spatial interaction between PVDF molecules and nanoparticle surfaces predominated in the crystallization behavior and morphology of the PVDF membrane. In the PTFE addition membrane, a predominant nucleation effect on the crystallization of PVDF accompanied by the S-L phase separation during the TIPS process led to a lamellar structure, whereas the MMT addition not only facilitated the lamellar crystals formation but also favored β phase crystal formation, because of the interactions between the surface of MMT and PVDF chains. Because of the nucleation effect, the crystallization temperature for PTFE addition mixture was higher than that for the mixture without nanoparticles, but the equilibrium melting temperature T_m^0 did not change significantly, except for the MMT addition mixture. In the MMT addition mixture, a double melting peak was observed. The lower one referred to the α phase, which was similar to other mixtures and the higher one referred to the β phase with the highest value of T_m^0.

The pore size of the membranes for both MMT and PTFE addition were very similar but smaller than that for the membrane without addition of nanoparticles. Because of the interconnected lamellar structure formed in the MMT and PTFE addition membranes, a higher tensile strength was obtained compared with that for the one without nanoparticles addition. Especially for the MMT addition membrane, the highest elongation at break was obtained, as a result of the β phase of PVDF crystal formed. This increased mechanical strength is thought highly beneficial for membrane development.

ACKNOWLEDGMENTS

This work was supported by the National Basic Research Program of China (973 Program) (2009CB623401), the National High Technology Research and Development Program of China (863 Program) (2009AA062901, 2012AA03A604), and the Major Program of Beijing Municipal Natural Science Foundation (2100001).

REFERENCES

1. Bottino, A.; Camera-Roda, G.; Capannelli, G.; Munari, S. *J. Membr. Sci.* **1991,** *57*, 1.
2. Su, Y. S.; Kuo, C. Y.; Wang, D. M.; Lai, J. Y.; Deratani, A.; Pochat, C.; Bouyer, D. *J. Membr. Sci.* **2009,** *338*, 17.
3. Lloyd, D. R.; Kim, S. S.; Kinzer, K. E. *J. Membr. Sci.* **1991,** *64*, 1.
4. Lloyd, D. R.; Kinzer, K. E.; Tseng, H. S. *J. Membr. Sci.* **1990,** *52*, 239.
5. Castro, A. J. U.S. Pat. 4,247,498 (**1981**).
6. Burghards, W. R. *Macromolecules* **1989,** *22*, 2482.
7. Matsuyama, H.; Teramoto, M.; Kudari, S.; Kitamura, Y. *J. Appl. Polym. Sci.* **2001,** *82*, 169.
8. Lloyd, D. R.; Kinzer, K. E.; Tseng, H. S. *J. Membr. Sci.* **1990,** *52*, 239.
9. Kim, L. U.; Kim, C. K. *J. Polym. Sci. Part B: Polym. Phys.* **2006,** *44*, 2025.
10. Tao, H. J.; Zhang, J.; Wang, X. L.; Xu, J. H. *J. Polym. Sci. Part B: Polym. Phys.* **2007,** *45*, 153.
11. Roh, I. J.; Ramaswamy, S.; Krantz, W. B.; Greenberg, A. R. *J. Membr. Sci.* **2010,** *362*, 211.
12. Gu, M. H.; Zhang, J.; Wang, X. L.; Ma, W. Z. *J. Appl. Polym. Sci.* **2006,** *102*, 3714.
13. Gu, M. H.; Zhang, J.; Wang, X. L.; Tao, H. J. *Desalination* **2006,** *192*, 160.
14. Su, Y.; Chen, C. X.; Li, Y. G.; Li, J. D. *J. Macromol. Sci. Part A: Pure Appl. Chem.* **2007,** *44*, 99.
15. Magalhães, R.; Durães, N.; Silva, M.; Silva, J.; Sencadas, V.; Botelho, G.; Gómez Ribelles, J. L.; Lanceros-Méndez, S. *Soft Mater.* **2010,** *9*, 1.
16. California, A.; Cardoso, V. F.; Costa, C. M.; Sencadas, V.; Botelho, G.; Gómez-Ribelles, J. L.; Lanceros-Mendez, S. *Eur. Polym. J.* **2011,** *47*, 2442.
17. Gu, M. H.; Zhang, J.; Xia, Y.; Wang, X. L. *J. Macromol. Sci. Part B: Phys.* **2008,** *47*, 180.
18. Lin, Y. K.; Tang, Y. H.; Ma, H. Y.; Yang, J.; Tian, Y.; Ma, W. Z.; Wang, X. L. *J. Appl. Polym. Sci.* **2009,** *114*, 1523.
19. van de Witte, P.; Dijkstra, P. J.; van den Berg, J. W. A.; Feijen, J. *J. Membr. Sci.* **1996,** *117*, 1.
20. Ma, W. Z.; Chen, S. J.; Zhang, J.; Wang, X. L.; Miao, W. H. *J. Polym. Sci. Part B: Polym. Phys.* **2009,** *47*, 248.
21. Ma, W. Z.; Chen, S. J.; Zhang, J.; Wang, X. L.; Miao, W. H. *J. Appl. Polym. Sci.* **2009,** *111*, 1235.
22. Moriyama, Y. D.; Iruma, H. M. U.S. Pat. 5,022,990 (**1991**).
23. Li, X. F.; Lu, X. L. *J. Appl. Polym. Sci.* **2006,** *101*, 2944.
24. Ma, W. Z.; Wang, X. L.; Zhang, J. *J. Therm. Anal. Calorim.* **2011,** *103*, 319.
25. Ma, W. Z.; Wang, X. L.; Zhang, J. *J. Polym. Sci. Part B: Polym. Phys.* **2010,** *48*, 2154.
26. Yang, J.; Li, D. W.; Lin, Y. K.; Wang, X. L.; Tian, F.; Wang, Z. *J. Appl. Polym. Sci.* **2008,** *110*, 341.
27. Kim, S. S.; Lim, G. B. A.; Alwattari, A. A.; Wang, Y. F.; Lloyd, D. R. *J. Membr. Sci.* **1991,** *64*, 41.
28. Tao, H. J.; Zhang, J.; Wang, X. L.; Gao, J. L. *J. Polym. Sci. Part B: Polym. Phys.* **2007,** *45*, 153.
29. Maiti, P.; Nam, P. H.; Okamoto, M.; Hasegawa, N.; Usuki, A. *Macromolecules* **2002,** *35*, 2042.
30. Schneider, S.; Drujon, X.; Lotz, B.; Wittmann, J. C. *Polymer* **2001,** *42*, 8787.
31. Vo, L. T.; Giannelis, E. P. *Macromolecules* **2007,** *40*, 8271.
32. Yu, L.; Cebe, P. *J. Polym. Sci. Part B: Polym. Phys.* **2009,** *47*, 2520.
33. Ma, W. Z.; Chen, S. J.; Zhang, J.; Wang, X. L. *J. Macromol. Sci. Part B: Phys.* **2010,** *50*, 1.
34. Verdonck, E.; Schaap, K.; Thomas, L. C. *Int. J. Pharm.* **1999,** *192*, 3.
35. Gregorio, J. R. *J. Appl. Polym. Sci.* **2006,** *100*, 3272.
36. Davis, G. T.; McKinney, J. E.; Broadhurst, M. G.; Roth, S. C. *J. Appl. Phys.* **1978,** *49*, 4998.
37. Kobayashi, M.; Tashiro, K.; Tadokoro, H. *Macromolecules* **1975,** *8*, 158.
38. Gregorio, R., Jr.; Nociti, N. C. P. S. *J. Phys. D: Appl. Phys.* **1995,** *28*, 432.
39. Benz, M.; Euler, W. B. *J. Appl. Polym. Sci.* **2003,** *89*, 1093.
40. Gregorio, R., Jr.; Cestari, M. *J. Polym. Sci. Part B: Polym. Phys.* **1994,** *32*, 859.
41. Ma, W. Z.; Zhang, J.; Chen, S. J.; Wang, X. L. *Appl. Surf. Sci.* **2008,** *254*, 5635.
42. Shah, D.; Maiti, P.; Gunn, E.; Schmidt, D. F.; Jiang, D. D.; Batt, C. A.; Giannelis, E. P. *Adv. Mater.* **2004,** *16*, 1173.
43. Ramasundaram, S.; Yoon, S.; Kim, K. J.; Lee, J. S.; Park, C. *Macromol. Chem. Phys.* **2009,** *210*, 951.
44. Lopes, A. C.; Costa, C. M.; Tavares, C. J.; Neves, I. C.; Lanceros-Mendez, S. *J. Phys. Chem. C* **2011,** *115*, 18076.
45. Hoffman, J. D.; Weeks, J. J. *J. Res. Natl. Bur. Stand. A: Phys. Chem.* **1962,** *66*, 13.
46. Lee, J. C.; Tazawa, H.; Ikehara, T. *Polym. J.* **1998,** *30*, 327.
47. McGuire, K. S.; Lloyd, D. R.; Lim, G. B. A. *J. Membr. Sci.* **1993,** *79*, 27.